Laser Welding of High-Strength Galvanized Steels in a Gap-Free Lap Joint Configuration under Different Shielding Conditions

By designing the specific shielding conditions, completely defect-free lap joints of the galvanized steels in a lap joint configuration are achieved by a single laser beam without pre- and postweld processing

BY S. YANG, B. CARLSON, AND R. KOVACEVIC

ABSTRACT

It is a great challenge to laser weld zinc-coated steels in a gap-free lap joint configuration due to the formation of highly pressurized zinc vapor. In this study, different shielding conditions were designed to mitigate the highly pressurized zinc vapor. Argon, helium, the mixture of argon and carbon dioxide, and the mixture of argon and oxygen were selected as the shielding gases to study the effects of shielding conditions on weld quality. The introduction of a side shielding gas not only blew away the laser-induced plasma but also suppressed the instability of the molten pool caused by the highly pressurized zinc vapor. Under the optimal setting of shielding gas conditions, a stable keyhole was consistently formed that provided a channel to vent out the zinc vapor. Under this welding condition, the laser welding process was very stable. Consequently, a completely defect-free lap joint was achieved in a gap-free lap joint configuration. Experimental results demonstrated that this newly developed laser welding procedure was robust and cost effective, does not require pre- or postweld processing and can be directly applied in the industrial conditions. A high-speed CCD camera, assisted with a green laser as the illumination source, was used to monitor the behavior of the molten pool and the keyhole dynamics in real time. Energy-dispersive X-ray spectroscopy (EDS) experiments were carried out to analyze the chemical compositions in the welds. Furthermore, tensile shear tests and microhardness measurements were conducted to evaluate the mechanical properties of the welds.

Introduction

In order to reduce fuel consumption, enhance passenger safety, and improve corrosion resistance, different grades of high-strength galvanized steels are increasingly used in the automotive industry. In the past, the high-strength galvanized steels used in the automotive industry were commonly joined with resistance spot welding. Considering the high speed, low heat input, deep penetration, and high flexibility of laser beam welding, the automotive industry has shown significant interest in applying high-powered lasers to joining galvanized steels. However, it is difficult to achieve a high-quality weld of galvanized steels in a lap joint configuration with using a single laser beam because of the presence of highly pressurized zinc vapor. The boiling point of zinc is 906°C, which is lower than the melting point of steels (over 1500°C). During laser welding of galvanized steels in a gap-free lap joint configuration, the highly pressurized zinc vapor is easily developed at the interface of the two metal sheets. The highly pressurized zinc vapor expels the liquid metal out of the molten pool and produces weld defects such as spatter and porosity during the laser welding process. These defects significantly degrade the mechanical properties of the weld joints.

In the past several decades, many efforts have been made to suppress the effect of the highly pressurized zinc vapor on the weld quality. The American Welding Society requires complete removal of the zinc coating layer at the interface of two metal sheets along the weld interface prior to laser welding (Refs. 1, 2). Currently, setting a small gap between the two metal sheets is a common way for industries to join the galvanized steels in a lap joint configuration (Ref. 3). Mazumder et al. (Refs. 4–6) developed a technique of alloying the zinc with the copper before the steel is melted. The melting point of the copper-zinc compound is 1083°C (between the melting temperature of steel and the boiling temperature of zinc). However, the solubility of copper into the steel could lead to additional problems such as hot cracking and corrosion (Ref. 7). Redesigning the lap joint to allow the zinc vapor to be evacuated, prior to the molten pool reaching the interface of the two metal sheets, has been explored in order to mitigate the effect of the zinc vapor (Refs. 8–11). In addition, Pennington et al. (Refs. 12, 13) proposed to deposit a nickel coating along the weld interface after stripping off the zinc coating at the interface of two metal sheets. The nickel has a melting point of 1453°C, which is higher than the boiling point of zinc. By replacing the zinc coating with a nickel coating in the weld area, the laser welding process becomes stable and accompanied by an associated corrosion protection. Unfortunately, this method will impose additional cost and reduce productivity. Pulsed laser (Ref. 14), dual laser beam or two lasers (Refs. 15–20), and hybrid laser welding

S. YANG (david.s.yang@gm.com) *is senior researcher, GM China Science Lab, Shanghai, P.R. China. B. CARLSON is lap group manager, General Motors R&D, Warren, Mich., and R. KOVACEVIC is professor, Mechanical Engineering, Southern Methodist University, Dallas, Tex.*

KEYWORDS

Galvanized Steels
Gap-Free Lap Joint Configuration
Laser Beam Welding
Keyhole
Shielding Conditions

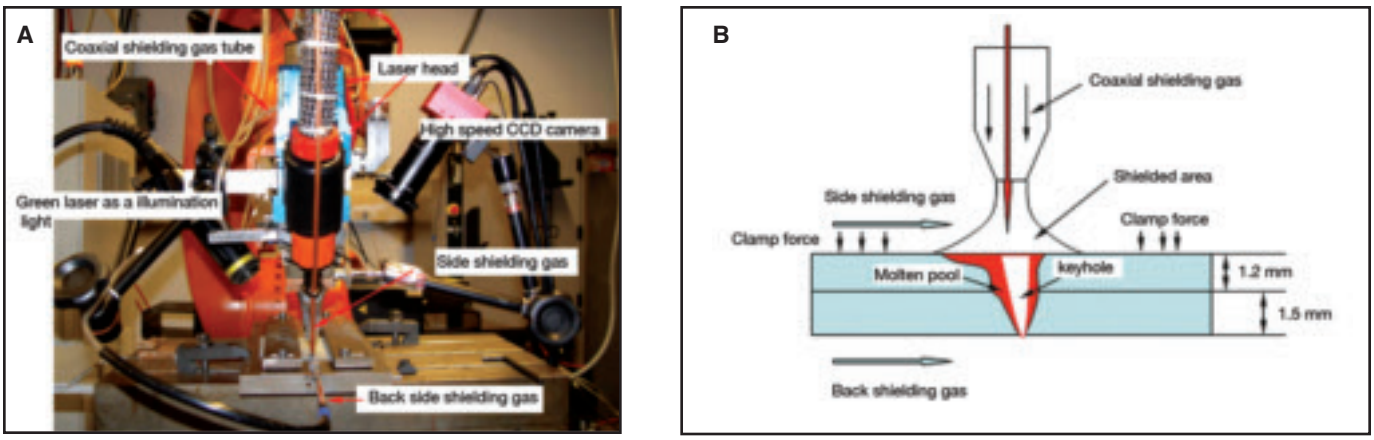

Fig. 1 — A — Experimental setup; B — schematic representation of lap joint configuration.

(Refs. 21–24) were also used to weld galvanized steels in a gap-free lap joint configuration. Gualini et al. (Ref. 18) modified the dual beam to join the galvanized steel sheets in a gap-free lap joint configuration where the first beam cut a slot to provide an exit path for the zinc vapor and the second beam was applied to join the metal sheets. However, experimental results demonstrated that spatter and porosity were still present in the lap joints. The laser-arc hybrid welding technique was also used by Kim et al. (Ref. 24) to join SGCD1 galvanized low-strength steel with a 1.0-mm thickness in a gap-free lap joint configuration. It was revealed that the formation of porosity was the main concern when using hybrid laser-arc welding of galvanized steels. In addition, they showed that process instability was the main cause of the generation of spatter and porosity in the welds. Spatter significantly damaged the torch electrode and the porosity lowers the mechanical properties of the welds. Additionally, Gu et al. (Ref. 25) also introduced the arc into the laser welding process where two heat sources share the common molten pool. They claimed that the arc enlarges the molten pool providing more space for the zinc vapor to escape. However, spatter and porosity were still observed in the welds. Recently, a method was proposed and patented by Li et al. (Refs. 26, 27) in which a thin aluminum foil layer was placed along the weld interface at the interface of two galvanized steel sheets to form an Al-Zn alloy during the laser welding process. They claimed that the level of the zinc vapor pressure was decreased through the formation of the Al-Zn alloy. In order to achieve high-quality lap joints, the two metal sheets should be tightly clamped. Li et al. (Ref. 27) claimed that if a gap existed at the interface of two metal sheets, weld defects would be produced in the welds. Furthermore, the weld became brittle due to the dissolution of aluminum-steel alloy into the weld. Recently, Yang and Kovacevic (Ref. 28) proposed a new welding procedure, which is a combination of a fiber laser with a gas tungsten arc welding (GTAW) torch used to preheat the top surface of the galvanized metal sheets. The GTAW preheating process burns the zinc coating at the top surface of the metal sheet, which helps in generating a thin film of the metal oxides (Ref. 28). The heated surface with the thin film of metal oxides will drastically improve the absorption of laser beam energy into the welded material. Furthermore, the zinc coating at the interface of the two metal sheets is transformed into zinc oxides, which has a higher melting point (above 1900°C) than that of steel (over 1500°C) resulting in less vapor generation and a more stable welding process. A completely defect-free, high-strength lap joint was achieved. However, this process requires a specific offset between the laser beam and GTAW torch that could hinder the application of this welding procedure in a highly automated welding application. The automotive industry continues to search for a new laser welding procedure to weld high-strength galvanized steels in a gap-free lap joint configuration with a single laser beam without the pre- and/or postweld processing requirements. Until now, there is no reference in the open literature on using a single laser beam to successfully join galvanized steels in a gap-free lap configuration without the pre- and/or post-processing requirements. Therefore, it is important to develop an efficient and robust laser welding technique to satisfy the demand from the automotive industry. The main objective of this work was to respond to this demand and develop a cost-effective and easy-to-automate laser welding technique.

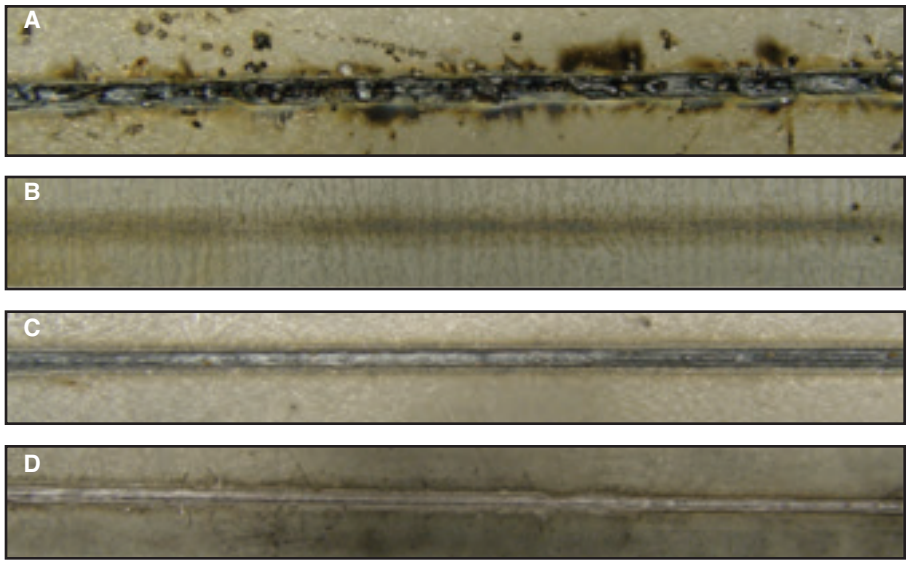

Fig. 2 — Lap joints obtained in Experiments 1 and 2: A — Top view of the lap joint obtained in Experiment 1; B — bottom view of the lap joint obtained in Experiment 1; C — top view of the lap joint obtained in Experiment 2; D — bottom view of the lap joint obtained in Experiment 2.

In this study, the laser welding process was conducted to join galvanized DP980 steel sheets in a gap-free lap joint config-

Table 1 — Laser Welding Parameters

No.	Coaxial Shielding Gas		Side Shielding Gas		Back Shielding Gas (ft^3/h)		Laser Power (W)	Welding Speed (mm/s)
	Type	Flow rate (ft^3/h)	Type	Flow rate (ft^3/h)	Type	Flow rate (ft^3/h)		
1	Ar	30			Ar	30	3600	40
2	He	30			Ar	30	3600	40
3	Ar	30	Ar	30	Ar	30	3600	40
4	He	30	Ar	30	Ar	30	3600	40
5	75% Ar+25% CO_2	30	Ar	30	Ar	30	3600	40
6	98% Ar+2% O_2	30	Ar	30	Ar	30	3600	40
7	90% Ar+10% CO_2	30	Ar	30	Ar	30	3600	40
8			Ar	20	Ar	30	3600	40
9			Ar	30	Ar	30	3600	40
10			Ar	40	Ar	30	3600	40
11	Ar	30	Ar	30	Ar	30	3600	30
12	Ar	30	Ar	30	Ar	30	3600	50
13	Ar	30	Ar	30	Ar	30	3600	60

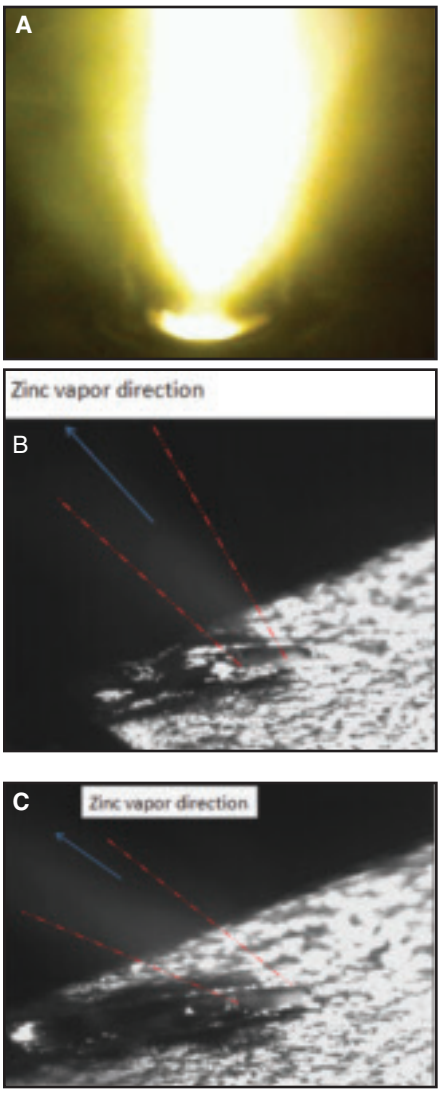

Fig. 3 — Unstable zinc vapor and laser-induced plume: A — Taken with color CCD camera at 30f/s; B and C taken with high-speed camera at 4000f/s assisted with a green laser.

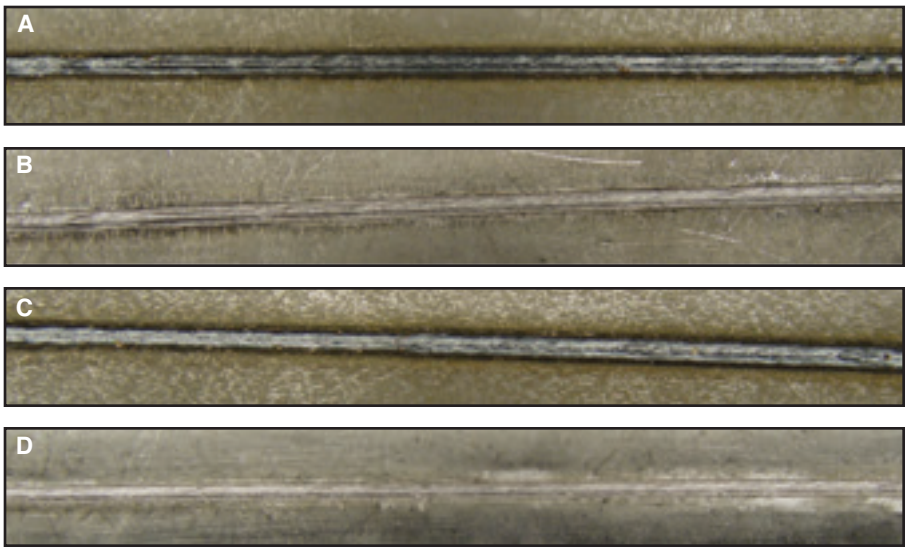

Fig. 4 — Effect of side shielding gas on the stability of the welding process and keyhole: A — Top view of the lap joint obtained in Experiment 3; B — bottom view of the lap joint obtained in Experiment 3; C — top view of the lap joint obtained in Experiment 4; D — bottom view of the lap joint obtained in Experiment 4.

uration. As shielding gas has a significant effect on the stability of the welding process and the weld quality (Refs. 29–31), the gases, including pure argon, helium, and carbon dioxide as well as oxygen, were combined in different ways to study the influences of the shielding conditions on the weld quality and the keyhole stability. An optimal shielding condition was proposed for the welding of galvanized steels in a gap-free lap joint configuration. The mechanism of stabilizing the laser welding process was studied. In addition, a high-speed CCD camera with the frame rate of 4000 f/s was used for on-line monitoring of the dynamic behavior of the molten pool and the laser-induced plasma. Energy-dispersive X-ray spectroscopy (EDS) tests were carried out to determine the chemical composition at the top surface as well as along the fusion zone of the welds. Microhardness and tensile shear tests were carried out to evaluate mechanical properties of the welds.

Experimental Setup

The material used in this study was galvanized DP 980 steel sheet. The zinc coating was hot dipped at the level of 60 gm/m^2 per side. Specimens with the dimensions of 200 × 85 × 1.2 mm and 200 × 85 × 1.5 mm were cut using an abrasive water jet. The 1.2-mm-thick metal sheet was selected as the top sheet and the 1.5-mm-thick metal sheet as the bottom sheet. The two metal sheets were then tightly clamped together during the laser welding process and a zero

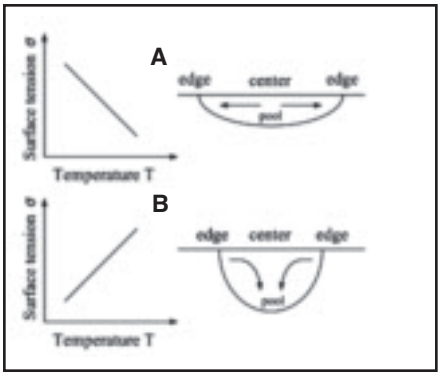

Fig. 5 — Effect of active gases on the Marangoni convection pattern by the surface tension gradient in the molten pool: A — The outward pattern; B— the inward pattern (Ref. 36).

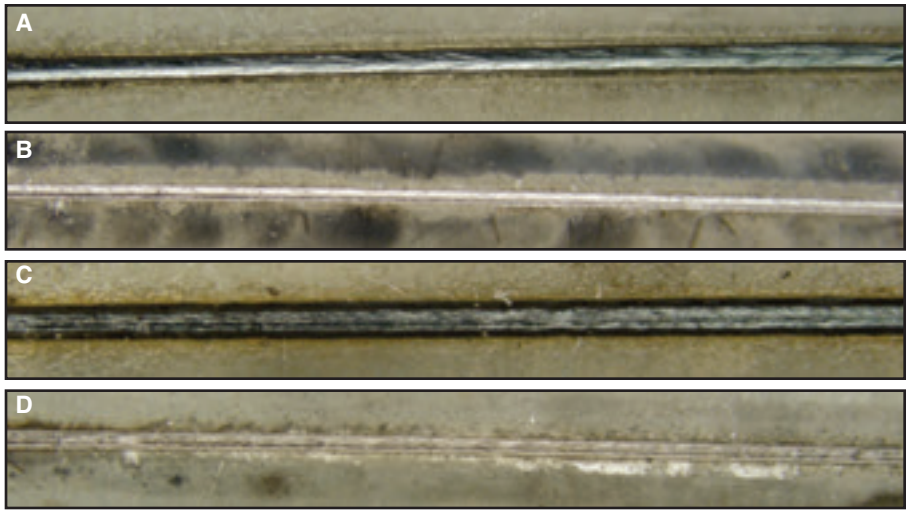

Fig. 6 — Effect of the active gas on the stability of the welding process and keyhole. A — Top view of the lap joint obtained in Experiment 5; B — bottom view of the lap joint obtained in Experiment 5; C — top view of the lap joint obtained in Experiment 6; D — bottom view of the lap joint obtained in Experiment 6.

gap was assumed. The laser welding process was performed using a 4000-W fiber laser. The multimode laser beam was brought into the laser welding head by an optical fiber with a core diameter of 0.4 mm. The laser welding head provided a laser beam focused to a 0.6-mm spot with a focal length of 250 mm. During the laser welding process, the laser beam was focused on the top surface of the two-sheet stack-up. A high-speed CCD camera with 4000 f/s and a color CCD camera with 30 f/s was applied to monitor the laser welding process. In addition, a CCD color video camera was used to monitor the laser-induced plasma and plume. The chemical compositions of base metal and weld zone were analyzed by EDS. A green laser with the center wavelength of 532 nm and a maximum output power of 6 W was selected as the illumination source to suppress the laser-induced plume in order to obtain clear images of the molten pool. Furthermore, the influence of the shielding conditions on the weld quality was evaluated using different combinations of the coaxial, side, and back shielding gases. The distance between the side shielding gas outlet (Fig. 1) and the laser spot was about 10~20 mm. In order to investigate the effect of the coaxial shielding gas on the welding quality, pure argon and helium, and the mixtures of argon and 25% and 10% CO_2, as well as the mixture of argon and 2% O_2 were used as the coaxial shielding gas in different welding experiments while maintaining all other welding parameters constant. Similarly, two kinds of gases, pure argon and pure helium, were selected as the side shielding gas to study the effect of the side shielding gas on weld quality in a sequence of experiments on the condition that all other welding parameters were kept constant. Table 1 presents the combinations of different gases and the laser welding parameters used in this study. The experimental setup is shown in Fig. 1. In addition, the lap joint coupons were sectioned, ground, polished, and etched for hardness measurement and examination under the optical microscope.

Results and Discussion

Investigation on the Effect of Different Shielding Conditions on Weld Quality

To study the effect of different coaxial shielding gases on the welding quality, pure argon and pure helium were used as the coaxial shielding gas in Experiments 1 and 2, respectively. In addition, the pure argon gas was used as the back shielding gas in Experiments 1 and 2. No side shielding gas was provided in these two experiments. Figure 2 shows the top and bottom views of the laser-welded lap joints obtained in Experiments 1 and 2. As shown in Fig. 2A, a large amount of spatter and porosity were produced in the laser-welded lap joints in Experiment 1. The spatter scattered along the laser-beam-delivered path will absorb and block a portion of the laser beam energy. However, when the coaxially delivered shielding gas was switched from pure argon to pure helium and the back shielding gas was maintained as pure argon (in Experiment 2), the laser welding process became very stable and no liquid metal was ejected from the molten pool. A sound weld with complete penetration was achieved with helium, as shown in Fig. 2C and D. The large difference in the weld quality between the shielding conditions specified by Experiments 1 and 2 was a result of the different ionization potentials of argon and helium. Helium has higher ionization potential and better thermal conductivity than that of argon (Ref. 32). When helium was used as the coaxial shielding gas, the size of plasma was small and stable (Ref. 32), and the laser beam energy could be better coupled into the welded material resulting in the formation of a stable keyhole. The presence of a stable keyhole will provide the channel to consistently vent out the highly pressurized zinc vapor. However, when the coaxially delivered shielding gas was argon and no side shielding gas was utilized, a large volume of the laser-induced plasma was directly formed on top of the molten pool, as shown in Fig. 3. As shown in Fig. 3, the laser-induced plasma is very unstable and dynamically fluctuated over time when argon was used as the shielding gas (Ref. 28). The unstable laser-induced plasma not only significantly influences the coupling efficiency of laser beam energy into the welded material but also changes the direction and size of the keyhole (Ref. 34). Under this welding condition, the keyhole tends to collapse and the highly pressurized zinc vapor will be trapped into the molten material. As shown in Fig. 2B, only partial weld penetration was achieved in the lap joints obtained when argon was used as the shielding gas because the laser-induced plasma and the produced spatter absorbed, scattered, and blocked the laser beam energy. This fact suggests that it was

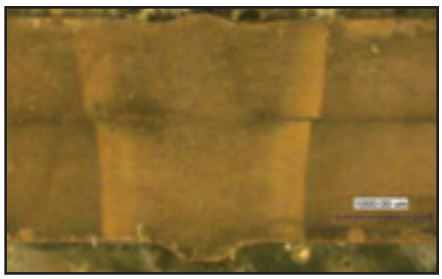

Fig. 7 — Cross-sectional view of the sound lap joints obtained in Experiment 4 (laser power: 3600 W; welding speed: 40 mm/s).

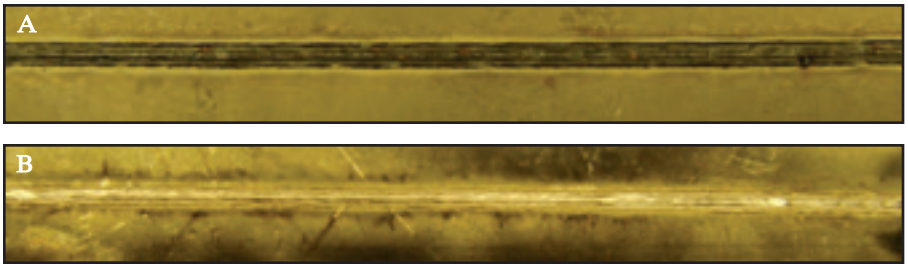

Fig. 8 — Lap joint obtained in Experiment 7: A — Top view; B — bottom view.

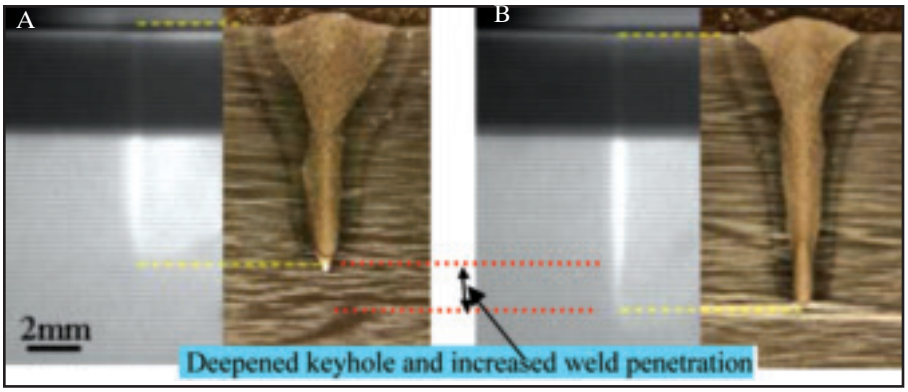

Fig. 9 — X-ray transmission images of keyhole and transverse sections for increased weld penetration by adding oxygen into the shielding gas (fiber laser power: 7 kW; welding speed: 1 m/min) (Ref. 43).

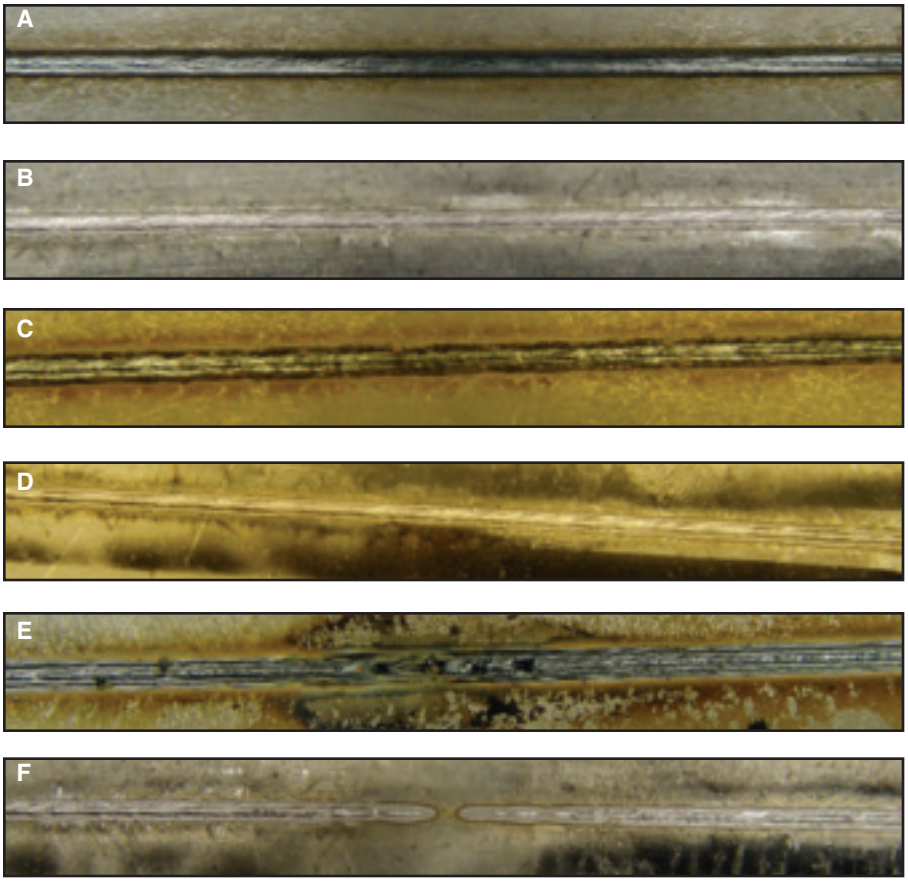

Fig. 10 — Lap joints obtained with different flow rates in Experiments 8–10: A — Top view of lap joints with a side flow rate of 20 ft³/h; B — bottom view of lap joints with a side flow rate of 20 ft³/h; C — top view of lap joints with a side flow rate of 30 ft³/h; D — bottom view of lap joints with a side flow rate of 30 ft³/h; E — top view of lap joints with a side flow rate of 40 ft³/h; F — bottom view of lap joints with a side flow rate of 40 ft³/h (laser power: 3600 W; welding speed: 40 mm/s).

critical to control the formation and stability of the laser-induced plasma in order to produce the stable keyhole for the laser welding process of galvanized steels in a gap-free lap joint configuration, thus achieving sound lap joints. The back side shielding gas can cool the weld to some extent to decrease the pressure level of zinc vapor because the zinc vapor pressure level is directly related to the temperature (Ref. 32). In general, when large amounts of spatter are produced, only partial penetration can be achieved.

As mentioned previously, the unstable plasma is one of the reasons for the collapse of the keyhole (Refs. 28, 34). Furthermore, the negative effects related to the unstable laser-induced plasma can be eliminated by applying a shielding gas with an approximate flow rate (Ref. 32, 34). In order to suppress the laser-induced plasma and achieve the stable keyhole, pure argon and pure helium were selected as the side shielding gases in Experiments 3 and 4, respectively. Figure 4 shows the experimental results. Neither spatter nor porosity were present in the laser welded lap joints and completely penetrated lap joints were achieved with both of these laser welding processes. This fact indicates that the laser welding process of galvanized steels was stabilized by the introduction of the side shielding gas. During the laser welding process, the side shielding gas will blow away the laser-induced plasma and plume. Furthermore, the use of side shielding gas stabilized the turbulent molten pool caused by the highly pressurized zinc vapor resulting in the flat surface of the welds (Refs. 30, 34), which will be shown in the following section by the high-speed camera. Compared with Experiment 1, the absorption efficiency of the laser beam energy was increased and the laser beam was relatively uniform enabling it to be coupled into the welded material and generate a stable keyhole. Similar to Experiment 2, the stable keyhole mitigates the highly pressurized zinc vapor.

Marangoni convection driven by the surface tension gradients is one of the main factors to influence the keyhole shape and its dynamics (Ref. 35). It has been revealed that the addition of active gases such as O_2 and CO_2 into the argon shielding gas can change the Marangoni convection from outward to inward, as shown in Fig. 5 (Ref. 36). In addition, the surface tension of a molten pool can be lowered (Ref. 37). The outward and inward Marangoni convection are shown in Fig. 5. When active gases such as O_2 or CO_2 are introduced into the shielding gas, it is possible to deepen and enlarge the keyhole, compared with the case using pure inert gas as the shielding gas (Ref. 37). In order to investigate whether adding the active gases O_2 or CO_2 into the inert gas could facilitate formation

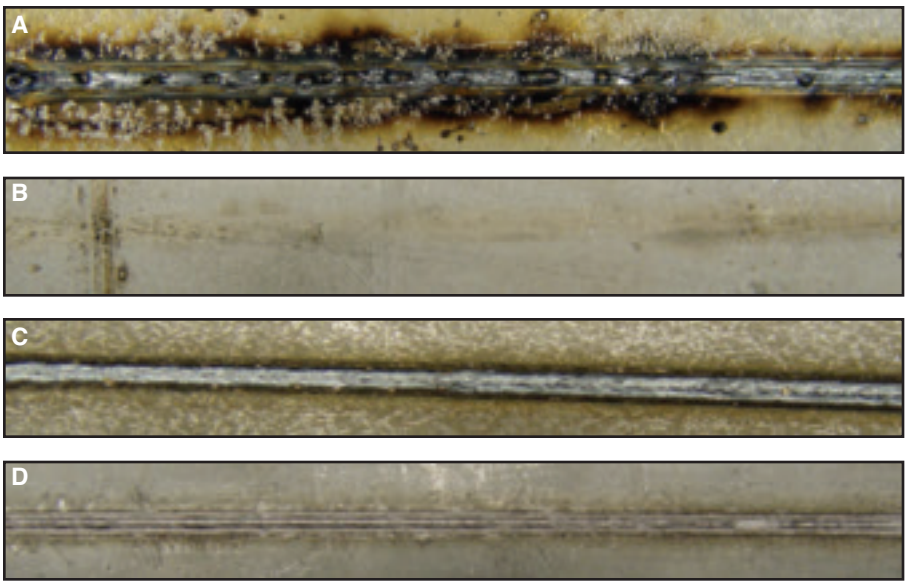

Fig. 11 — The lap joints obtained at different welding speeds in Experiments 12 and 13: A — Top view of lap joint obtained at 60 mm/s welding speed; B — bottom view of lap joint at 60 mm/s welding speed; C — top view of lap joint obtained at 50 mm/s welding speed; D — bottom view of lap joint at 50 mm/s welding speed (laser power: 3600 W).

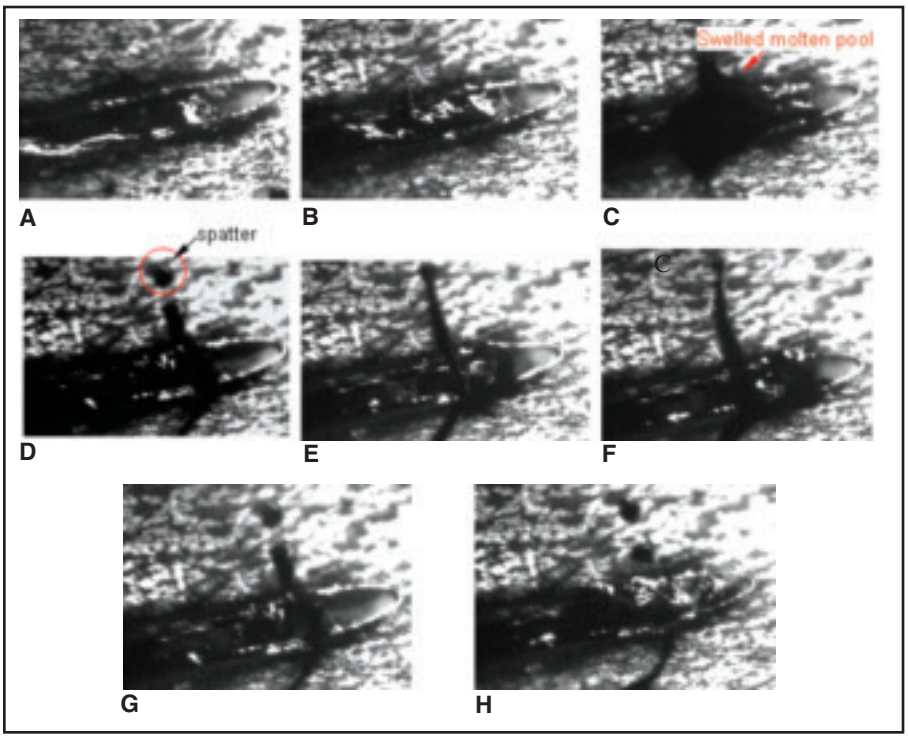

Fig. 13 — Images of the molten pool successively obtained with the unstable laser welding process (laser power: 3600 W; welding speed: 40 mm/s; the pure argon shielding gas used in the coaxial and back sides).

of the keyhole and enhance its stability for laser welding of galvanized steels in a gap-free lap joint configuration, the mixture of argon + CO_2 and argon + O_2 was further tested in Experiments 5–7. The high CO_2 or O_2 content in the shielding gas may decrease the mechanical properties of welds (Ref. 30). When welding steel, the percentage of O_2 and CO_2 in the inert shielding gas is recommended to be no more than 25% in order to maintain the same properties in the weld as the base material (Ref. 38). In addition, the mixture of 98% argon and 2% O_2 is commonly used in industry for welding steel. Therefore, the mixtures of 75% Ar + 25% CO_2 and 98% Ar + 2% O_2 were used in the experiments. Figure 6 shows the experimental results. As shown in Fig. 7, high-quality welds with complete penetration were achieved. Figure 7 shows the cross-sectional view of the lap joints obtained in Experiment 5. As shown in Fig. 7, no porosity is present in the lap joints.

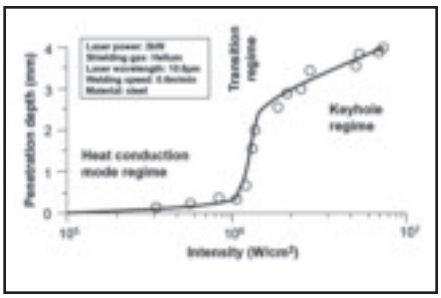

Fig. 12 — Penetration depth vs. intensity for laser beam welding process (Ref. 47).

By direct observation of the laser welding process, it was found that the welding process in Experiment 5 with the mixture of 75% Ar + 25% CO_2 was the most stable among all the gas mixtures tested. In addition, the laser welding processes in Experiments 4 and 6 exhibited a more stable process than that of Experiment 3. When using pure argon as the coaxial shielding gas in Experiment 3, the welding process was slightly unstable and a small amount of spatter was observed during the laser welding process. More severely, some porosity was produced in the welds, suggesting that when the coaxially delivered shielding gas contains either CO_2 or O_2 or is pure helium, the laser welding process obtains the greatest degree of stability. Therefore, it is recommended to introduce CO_2 or O_2 gas into the shielding gases or use pure helium or the mixture of He and Ar instead of pure argon to stabilize the laser welding process for galvanized steels. Trials were also carried out to join the galvanized steels in a gap-free lap joint configuration with 90% Ar + 10% CO_2. Figure 8 shows the experiment results. As shown in Fig. 8, complete penetration was achieved and the weld bead was continuous without the presence of spatter or porosity. Further studies will be performed to explore the process window for different gas ratios in different shielding conditions.

Mechanism for Enhanced Stability of the Laser Welding Process by the Introduction of Active Gases

As discussed in the previous section, the introduction of an active gas (O_2 or CO_2) into the shielding gas can suppress the highly pressurized zinc vapor and stabilize the laser welding process. During laser welding of galvanized steels, the active gases play these possible roles as follows:

1. During the laser welding process, dissociation and ionization processes take place in the gases (Ref. 39). The chemical reaction between Zn vapor and the active

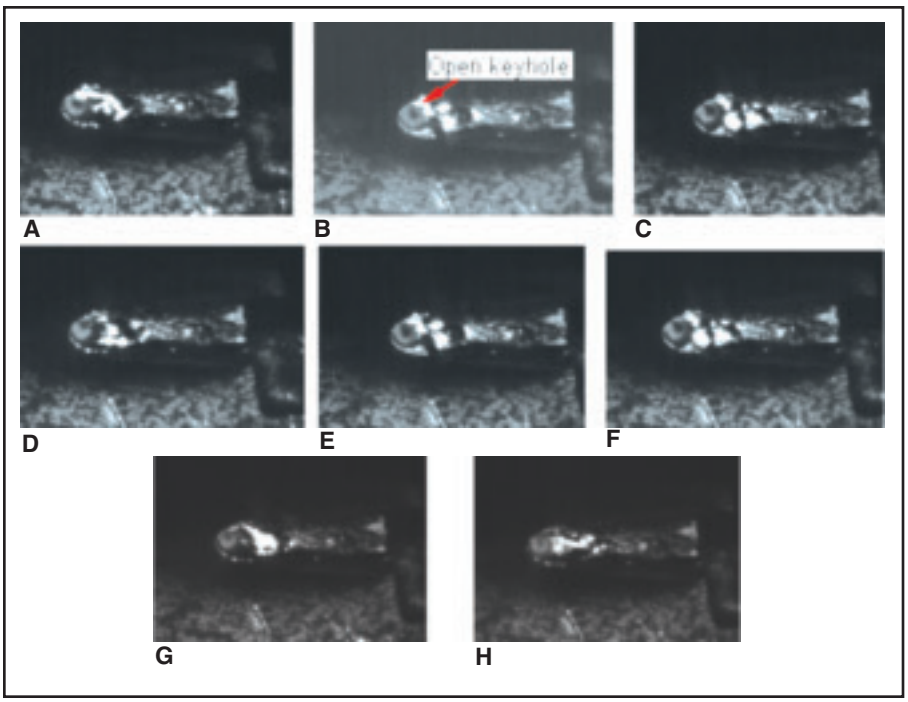

Fig. 14 — The images of the molten pool successively obtained in the stable laser welding process (laser power: 3600 W; welding speed: 40 mm/s; the coaxial 90% Ar +10% CO_2 shielding gas: 30 ft^3/h; the back and side pure argon shielding gas: 30 ft^3/h).

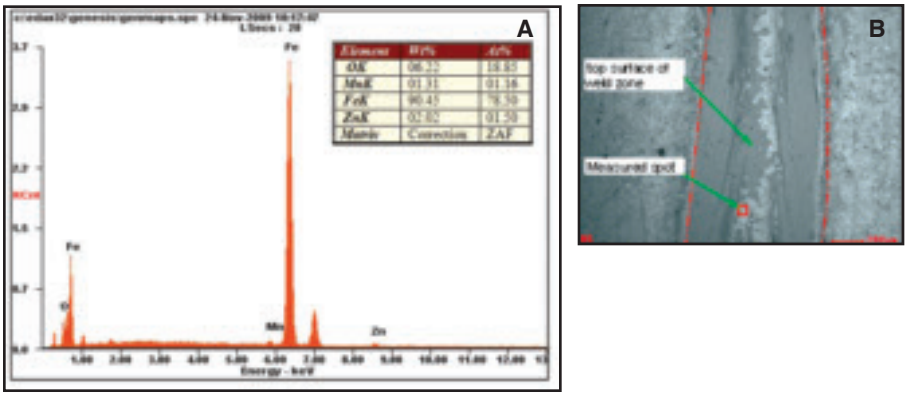

Fig. 15 — EDS analysis of the top surface of weld; A — EDS result in the measured spot; B — SEM image of the top surface of weld. Welds obtained by the following welding parameters: Laser power, 3600 W; welding speed, 40 mm/s; the coaxial shielding gas, 30 ft^3/h of the mixture of 75% Ar + 25% CO_2; back and side shielding gas, 30 ft^3/h of pure argon.

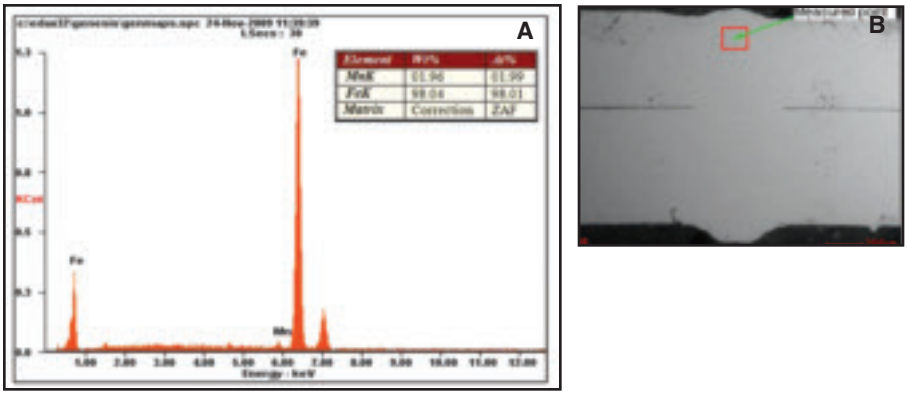

Fig. 16 —EDS analysis of the cross section of the weld: A — EDS result in the measured spot; B — SEM image of the cross section of the weld.

gases O_2 and CO_2 will form ZnO according to $2Zn + O_2 \rightarrow ZnO$ and $CO_2 \rightarrow C + O_2 \rightarrow Zn + O \rightarrow ZnO$. This chemical reaction could help stabilize the welding process.

2. A thin film of metal oxides (mainly iron oxides) could form in the front of the molten pool. The formation of metal oxides as well as heated surface material increased the coupling efficiency of laser beam energy into the welded material (Refs. 40, 41). Under this condition, the keyhole was readily formed, which provided the channel for the highly pressurized zinc vapor to be vented out. When the surface tension had an outward pattern, weld penetration was shallow (Ref. 42). Inversely, deep weld penetration can be obtained when the surface tension has an inward pattern. By introduction of active shielding gases such as O_2 and CO_2, the surface tension changed from an outward pattern to an inward pattern (Ref. 43). Consequently, the keyhole was enlarged and deepened (Ref. 43), as shown in Fig. 9.

3. The viscosity of molten metal was decreased through introduction of active shielding gases such as O_2 and CO_2 in comparison with the laser welding experiments where pure argon was used as the shielding gas (Ref. 44). Therefore, the shear force exerted on the keyhole wall by the highly pressurized zinc vapor could be reduced. Thus, the potential for formation of spatter and porosity was subsequently reduced.

During the laser welding process, carbon dioxide can be dissociated into $CO + \frac{1}{2}O_2$ or $C + O_2$, depending upon the dissociation potential. If the dissociation potential is high enough, the CO is further transformed into $C + \frac{1}{2}O_2$. The large amount of carbon dissolving into the weld metal reduces the corrosion resistance of the low-carbon grades of steels (Ref. 45). Furthermore, the strength of the welds may be decreased by reducing the amount of deoxidating alloying elements such as manganese and silicon, which react with oxygen in the shielding gas (Ref. 45). In like manner, the addition of oxygen into the shielding gas may pose a risk for the reduction of the weld strength. Therefore, the issue on control of the percentage of CO_2 or O_2 in the shielding gas may be of concern when using the mixtures of $Ar + CO_2$ or $Ar + O_2$ in the shielding gas for laser welding of galvanized steels. On the other hand, since the laser welding process was carried out at the high welding speed, the cooling rate was fast. As a result, the interaction time between the carbon or oxygen and the deoxidizable alloys was extremely short such that the issues mentioned previously may not be of concern. Further studies are planned to explore these phenomena.

Influence of the Side Shielding Gas Flow Rate on Weld Quality

In order to study the influence of the

side shielding gas flow rate on the weld quality, laser welding experiments were carried out with shielding conditions as follows: no coaxial shielding gas, a constant 30 ft^3/h pure argon back shielding gas flow rate, pure argon side shielding gas flow rate varying from 20 to 40 ft^3/h. Figure 8 shows the experimental results on the weld quality. As shown in Fig. 8, no spatters or porosity were generated in the welds and complete penetration was achieved in the welds when the flow rate of the side shielding gas was 20 and 30 ft^3/h. When the flow rate of the side shielding gas was increased to 40 ft^3/h, the welding process became dramatically unstable and some spatter and porosity were produced in the welds, as shown in Fig. 10E. In addition, only partial penetration was achieved in the welds. This phenomenon can be explained by the fact that when the flow rate of the side shielding gas was increased to a sufficiently high level, the argon gas enabled the formation of more plasma when the laser beam penetrated through the argon gas than what laser-induced plasma was blown off for the given laser power and welding speed. It is worth mentioning that the argon side shielding gas can be replaced by another shielding gas such as helium to suppress the laser-induced plasma with the optimal flow rate to achieve a sound lap joint.

Influence of Welding Speed on Weld Quality

In order to study the influence of the welding speed on weld quality, three trial tests were conducted where the welding speed was varied from 30 to 60 mm/s in increments of 10 mm/s and all other welding parameters were identical to those in Experiment 4. Experimental results demonstrated that for a given laser power of 3600 W, a sound weld could be achieved at welding speeds of 30, 40, and 50 mm/s. However, the laser welding process tended to become unstable, producing spatter and porosity in the welds at the welding speed of 60 mm/s, as shown in Fig. 11. The instability of the laser welding process at 60 mm/s welding speed can be explained by the fact that when the welding speed was increased, the keyhole became unstable and tended to collapse (Ref. 46). Keyhole formation required that the laser beam energy density was beyond some threshold value (Ref. 47), as shown in Fig. 12. The energy density can be described by the following equation:

$$E_d = d * (P_d/V) \qquad (1)$$

where d is the focused spot size, P_d is the laser power at the focus point, and V is the welding speed. When the speed was increased, the energy density was decreased and the keyhole tended to collapse. The collapsed keyhole failed to vent out the highly pressurized zinc vapor, which led to

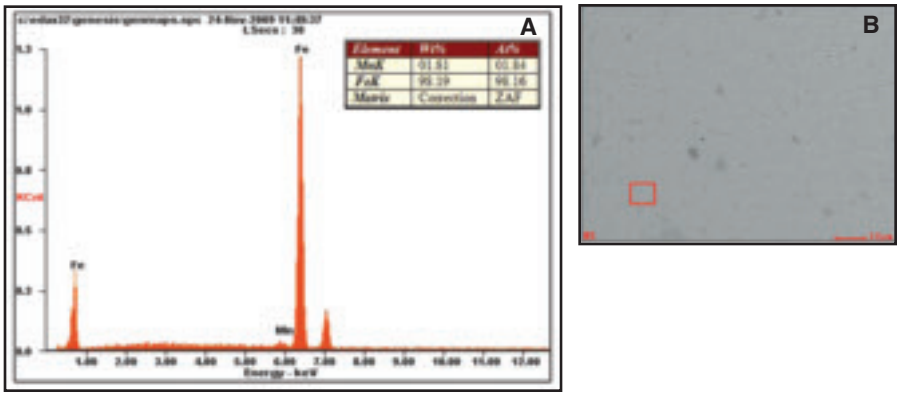

Fig. 17 — EDS analysis of the cross section of base material: A — EDS result in the measured spot; B — SEM image of the cross section of the base material.

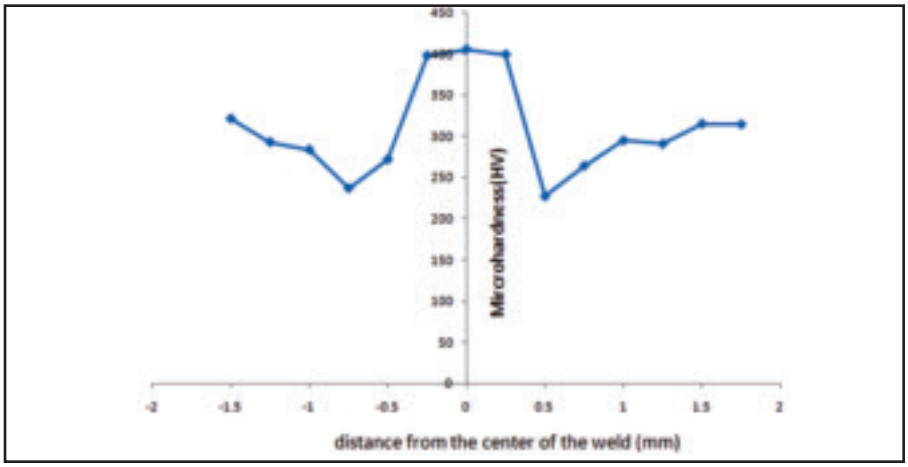

Fig. 18 — Microhardness profile of a weld. (Welds obtained in Experiment 6.)

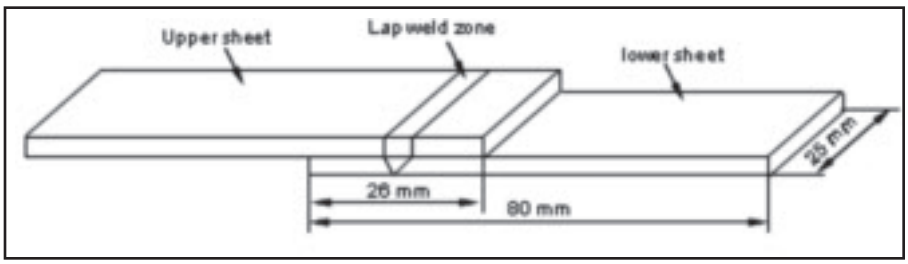

Fig. 19 — Schematic diagram of the geometry of the tensile shear test sample.

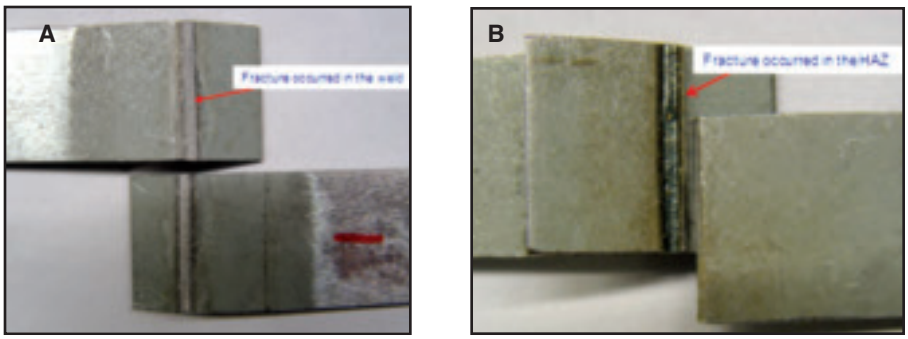

Fig. 20 — Failure location of the tensile shear test samples with different welding conditions: A — Tensile shear test fracture location of lap joints obtained in Experiment 5; B — tensile shear test fracture location of lap joints obtained in Experiment 7.

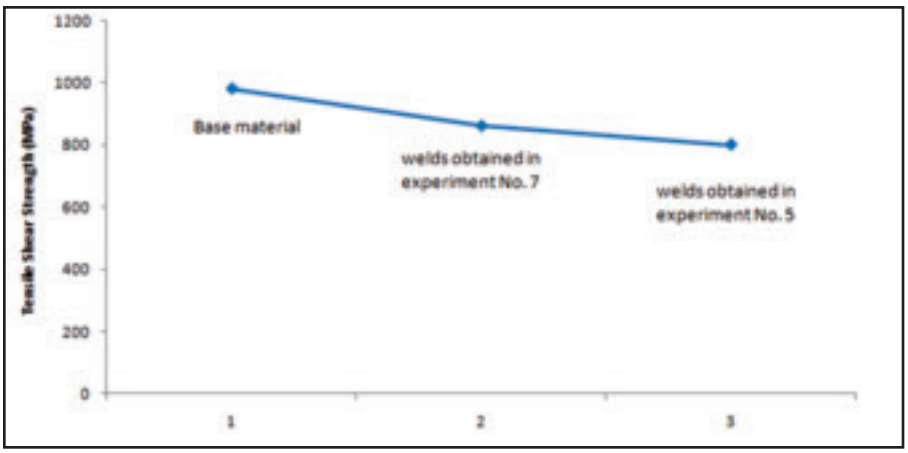

Fig. 21 — Tensile test results.

a large amount of spatter and porosity in the welds. The spatter flying in the laser beam path absorbed and reflected the laser beam energy. In addition, the multireflection will not occur in the collapsed keyhole. So, when the keyhole is collapsed, a relatively lower level of laser beam energy is absorbed by the welded material, resulting in partial penetration. Therefore, it is important to control welding speed for obtaining a stable keyhole. In addition, when welding speed was relatively lower, for the given laser power and shielding gas flow rate, it was more possible to achieve complete penetration. When complete penetration was achieved, a portion of the highly pressurized zinc vapor can escape from the bottom of specimens producing a more stable laser welding process.

Direct Observation of Dynamic Behaviors of the Molten Pool with the Machine Vision System

To study the behaviors of the molten pool and the keyhole dynamic, a high-speed (4000 f/s) CCD camera was applied to monitor the laser welding process in real time. Figures 13 and 14 show the molten pool and the keyhole obtained during the unstable and stable laser welding processes. During the unstable laser welding process, the keyhole has difficulty forming, as shown in Fig. 13. In addition, the molten metal flow in the rear part of the molten pool dramatically fluctuates over time. When the welding process was unstable, the highly pressurized zinc vapor developed at the interface of two metal sheets ejects the liquid metal out of the rear portion of the molten pool. This expulsive liquid metal condensed in the air and became spatter that was deposited on the weld surface or weld zone in random directions. A large amount of spatter not only damaged the optical lens but also produced poor quality lap joints and poor surface appearance. The presence of the spatter and porosity in the welds dramatically reduced the strength of the lap joints. In contrast, a stable keyhole was consistently formed and kept open during the entire laser welding process, which mitigates the highly pressurized zinc vapor, thus producing a stable laser welding process. As shown in Fig. 14, the keyhole appears as a black spot located in front of the molten pool. Due to the mitigation of zinc vapor through the stable open keyhole, the molten pool was stable and no liquid metal was rejected from it. Consequently, sound lap joints were achieved in the stable laser welding process. Furthermore, the coupling efficiency of laser beam energy into the welded material was enhanced by multireflection into the keyhole. Therefore, deep weld penetration is attained.

Energy-Dispersive X-Ray Spectroscopy (EDS) Analysis

In order to analyze the chemical elements of the weld and ensure that the use of high levels of CO_2 would not cause the loss of the alloying elements in the weld, energy-dispersive X-ray spectroscopy (EDS) experiments were carried out at different locations on the top surface and along the cross-sectional zone of the welds. Figures 15 and 16 present typical EDS analysis results at the measured points on the top surface and along the cross section of the weld. Figure 17 shows the EDS analysis results at the cross section of the base material. As shown in Fig. 15, the O, Fe, Mn, and Zn elements are presented in the EDS analysis results detected on the top surface of the weld. It is conjectured that the zinc oxide, iron oxides, and manganese oxide are probably produced on the top surface of the welds due to the dissociation of CO_2 into the formations of $CO + O_2$ or $C + O_2$. The oxides of ZnO, MnO, and FeO are produced according to the following reactions: $Zn + \frac{1}{2}O_2 \rightarrow ZnO$; $Fe + \frac{1}{2}O_2 \rightarrow FeO$; and $Mn + \frac{1}{2}O_2 \rightarrow MnO$. Furthermore, for all of the measured points in the cross section of the weld, the presence of Fe and Mn elements without the O element was identified from the peaks present in the EDS analysis results. Based on the absence of the oxygen element in the weld, the conclusion may be made that no oxygen contamination has occurred in the weld during the laser welding process with the introduction of oxygen and carbon dioxide. Based on the weight percentages of various elements in Figs. 16 and 17, the amount of the essential alloying element of Mn in the weld is not degraded during the laser welding process even if a high percentage of CO_2 is used in the coaxial shielding gas. This fact indicates that the issue of the loss of oxidizing alloy elements such as manganese may not be of concern for the high-speed laser welding process with the addition of carbon dioxide or oxygen into the coaxial shielding gas. However, further study is still required for the resistance test. Since the iron oxides can influence the metallurgical properties of welds (Ref. 39), the percentage of oxygen or carbon dioxide in the shielding gas mixture should be controlled in order to maintain the same chemical composition and mechanical properties of the welds as the base material.

Mechanical Tests

Vickers hardness measurements were conducted on a cross section of the weld along a line 0.25 mm under the top surface using a load of 200 g and a 10-s dwell time. Figure 18 shows the measured line and the hardness profiles across the weld zone and the heat-affected zone (HAZ) as well as the base material. The microhardness values are a function of the distance from the weld center. In the fusion zone, the weld has a higher hardness value than that of the base material due to the fast cooling. The hardness then decreases toward the fusion boundary. Because of the effect of softening, the HAZ is characterized by the lowest hardness value, lower than that in both the weld zone and the base material.

Tensile shear tests were performed to determine the strength of the welds. The sample geometry is shown in Fig. 19. The tensile shear strength is determined by the average value of two series of values taken on the same specimen welded under a specific set of welding parameters. The weld width at the interface measured from the weld cross section, which was changed by different welding conditions, was used to calculate the tensile strength. Figure 20 shows the weld fracture location after the tensile shear test. As shown in Fig. 20, both of the test specimens are broken under the shear force at the fusion zone, for a coaxial shielding gas mixture of 90% Ar + 10% CO_2. However, when the coaxial shielding

gas is switched to the mixture of 75% Ar + 25% CO_2 and the other welding parameters are kept the same as in the case of using the 90% Ar + 10% CO_2, the fracture of test samples happens in the HAZ, as illustrated in Fig. 20B. Figure 21 summarizes the tensile test results. The average shear strength for the welds obtained with the welding parameters in Fig. 20A is 860 MPa and the average tensile strength for the welds obtained with the welding parameters in Fig. 20B is 800 MPa. The strength of the base material is 980 MPa. Comparison of the strength of the welds with that of the base materials reveals that the strength is slightly reduced when using the mixtures of 75% Ar + 25% CO_2 and 90% Ar + 10% CO_2 as the shielding gases.

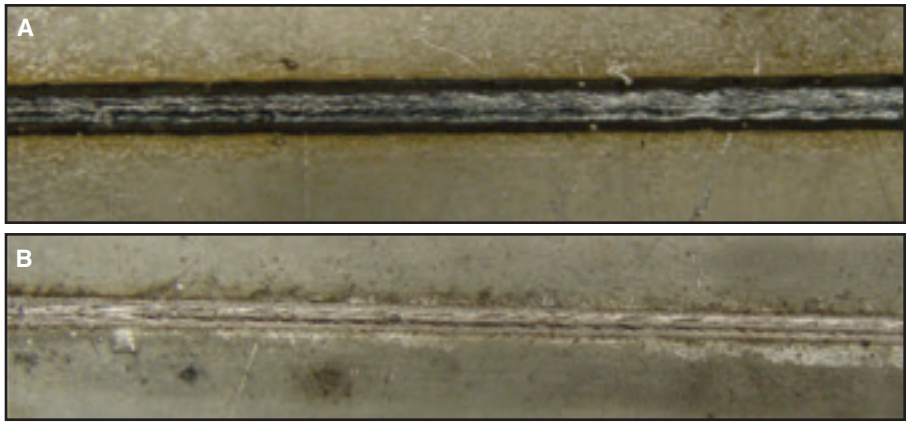

Fig. 22 — Completely defect-free laser-welded lap joint with a side shielding gas only: A — Top view; B — bottom view (laser power: 3600 W; welding speed: 30 mm/s; side shielding gas: pure argon; side shielding gas flow rate: 30 ft³/h).

Laser Welding of Galvanized Steels in a Gap-Free Lap Joint Configuration with a Single Side Shielding Gas

In order to study the influence of a single side shielding gas on the weld quality, a further trial test was conducted where the welding speed was 30 mm/s, laser power was 3600 W, the side shielding gas flow rate was 30 ft^3/h, and no back and coaxial shielding gases were used. As shown in Fig. 22, a sound lap joint with complete penetration was also achieved. No spatter and porosity were produced on the welds. Therefore, it is also possible to just use a single side shielding gas for laser welding of galvanized steels in a gap-free configuration to obtain sound lap joints. Further studies on the influences of side shielding gas composition, size/shape of the side shielding gas nozzle, distance of the side shielding gas nozzle from the keyhole, and the angle of the nozzle with respect to the plane of the top sheet on the weld quality are needed to be completed for a given welding speed and laser power. In this paper, we will not discuss these issues.

Conclusions

The following conclusions can be drawn from this work:

1. With the specific shielding conditions, a completely defect-free lap joint of galvanized steels in a gap-free configuration can be achieved by a single laser beam without pre- and postweld processing. The proposed laser welding procedure, which is robust, can be conducted at high speed to obtain completely penetrated, high-strength lap joints.

2. The introduction of the side shielding gas can not only suppress the laser-induced plasma and plume but also stabilize the turbulent molten pool caused by the highly pressurized zinc vapor resulting in a stable keyhole, which allows the highly pressurized zinc vapor to be vented out. With the formation of the keyhole, the absorption efficiency of laser beam is increased, and it is better coupled to the materials to be welded. It is not necessary to use the bottom shielding gas during the laser welding process.

3. The keyhole could be stabilized, enlarged, and deepened by the addition of active gases (O_2 and CO_2) during the laser welding process. Compared with the case of using pure argon, deeper penetration could be achieved when adding the active gas (O_2 and CO_2) into the shielding gas.

4. Lower travel speeds that results in complete penetration produced sound welds whereas the partial penetration weld made at the fastest travel speed was defective.

5. Alloying elements such as Mn are not reduced by the introduction of the active gas (O_2 and CO_2) into the coaxial shielding gas.

6. The fracture location of the welds varies from the fusion zone to the heat-affected zone (HAZ) during the tensile tests with an increase in the percentage of CO_2 in the mixture of argon + CO_2. In addition, the HAZ is softened during the laser welding process. Furthermore, EDS analysis results do not detect a loss of Mn in the weld during the laser welding process.

Acknowledgments

This work was funded by General Motors and NSF grant No. EEC-0541952. The authors acknowledge Andrew Socha, research engineer; Junjie Ma, PhD student; and Dr. Xinfeng Li, visiting scholar at Research Center for Advanced Manufacturing at Southern Methodist University for their assistance in performing the experiments.

References

1. Akhter, R., Steen, W. M., and Watkins, K. G. 1991. Welding zinc-coated steel with a laser and the properties of the weldment. *Journal of Laser Applications* 3(2): 9–20.

2. AWS WZC/D19.0-72, *Welding Zinc-Coated Steels*. Miami, Fla.: American Welding Society.

3. Graham, M. P., Hirak, D. M., Kerr, H. W., and Weckman, D. C. 1994. Nd:YAG laser welding of coated sheet steel. *Journal of Laser Applications* 6(4): 212–222.

4. Mazumder, J., Dasgupta, A., and Bembenek, M. 2002. Alloy based laser welding. U.S. Patent No. 6,479,168.

5. Dasgupta, A., Mazumder, J., and Bembenek, M. 2000. Alloying based laser welding of galvanized steel. *Proceedings of International Conference on Applications of Lasers and Electro Optics*, Laser Institute of America, Dearborn, Mich.

6. Dasgupta, A., and Mazumder, J. 2006. A novel method for lap welding of automotive sheet steel using high power CW CO_2 laser, *Proceedings of the 4th International Congress on Laser Advanced Materials Processing*.

7. Pieters, R. R. G. M., Bakels, J. G., Hermans, M. J. M., and den Ouden, G. 2006. Laser welding of zinc coated steels in an edge lap configuration. *Journal of Laser Applications* 18(3): 199–204.

8. Graham, M. P., Hirak, D. M., Kerr, H. W., and Weckman, D. C. 1994. Nd:YAG laser welding of coated sheet steel. *Journal of Laser Applications* 6(4): 212–222.

9. Sacks, J. L., Davis, H., and Spilchen, W. 2007. Corrosion resistant wire products and method of making same. U.S. Patent No. 20070119715.

10. Graham, M. P., Hirak, D. M., Kerr, H. W., and Weckman, D. C. 1996. Nd:YAG laser beam welding of coated steels using a modified lap joint geometry. *Welding Journal* 75(5): 162-s- to 170-s.

11. Graham, M. P., Hirak, D. M., Kerr, H. W., and Weckman, D. C. 1996. Laser welding of Zn-coated sheet steels. *Proceeding of SPIE: International Society for Optical Engineering*, V. 2703.

12. Pennington, E. J. 1987. Laser welding of galvanized steel, U.S. Patent No. 4642446.

13. Williams, S. W., Salter, P. L., Scott, G., and Harris, S. J. 1993. New welding process for galvanized steel. *Proc. 26th Int. Symp. Automotive Technology and Automation,* 49–56, Aachen, Germany.

14. Teng, Y. F. 1999. Pulsed Nd:YAG laser seam welding of zinc-coated steel. *Welding Journal* 78(7): 238-s to 244-s.

15. Forrest, M. G., and Lu, F. 2005. Development of an advanced dual beam head for

laser lap joining of zinc coated steel sheet without gap at the interface. *24th International Congress on Applications of Lasers and Electro-Optics*, ICALEO: 1069–1074.

16. Chen, W., Ackerson, P., and Molian, P. 2009. CO_2 laser welding of galvanized steel sheets using vent holes. *Material & Design*, Vol. 30, pp. 245–251.

17. Xie, J. 2002. Dual beam laser welding. *Welding Journal* 81(10): 223-s to 230-s.

18. Gualini, M. M. S., Iqbal, S., and Grassi, F. 2006. Modified dual-beam method for welding galvanized steel sheets in lap configuration. *Journal of Laser Applications* 18(3): 185–191.

19. Forrest, M. G., and Lu, F. 2005. Development of an advanced dual beam head for laser lap joining of zinc coated steel sheet without gap at the interface. *24th International Congress on Applications of Lasers and Electro-Optics*, pp. 1069–1074.

20. Milberg, J., and Trautmann, A. 2009. Defect-free joining of zinc-coated steels by bifocal hybrid laser welding. *Production Engineering Research Development*, Vol. 3, pp. 9–15.

21. Choi, H. W., Farson, D. F., and Cho, M. H. 2006. Using a hybrid laser plus GMAW process for controlling the bead humping defect. *Welding Journal* 85(8): 174-s to 179-s.

22. Mueller, G. H. 2004. Hybrid welding of galvanized steel sheet. European Patent EP 1454701.

23. Kusch, M., and Thurner, S. 2008. Application of the plasma-MIG technology for the joining of galvanized steel materials. *Welding and Cutting* 7(1): 54–59.

24. Kim, C., Choi, W., Kim, J., and Rhee, S. 2008. Relationship between the weldability and the process parameters for laser-TIG hybrid welding of galvanized steel sheets. *Materials Transactions* 49(1): 179–186.

25. Gu, H., and Mueller, R. 2001. Hybrid welding of galvanized steel sheet. *20th International Congress on Applications of lasers & Electro-Optics*, ICALEO: 13–19.

26. Li, X. G., Lawson, W. H. S., and Zhou, Y. N. 2008. Lap welding of steel articles having a corrosion resisting metallic coating. U.S. Patent No. 2008/0035615 A1.

27. Li, X., Lawson, S., and Zhou, Y. 2007. Novel technique for laser lap welding of zinc coated sheet steels. *Journal of Laser Applications* 19(4): 259–264.

28. Yang, S. L., and Kovacevic, R. 2009. Laser welding of galvanized DP 980 steel assisted by the GTAW preheating in a gap-free lap joint configuration. *Journal of Laser Application*, Vol. 21, No. 3, pp. 139–148.

29. Natio, Y., Mizutani, M., and Katayama, S. 2006. Effect of oxygen in ambient atmosphere on penetration characteristics in single yttrium-aluminum-garnet laser and hybrid welding. *Journal of Laser Applications*. Vol. 18, pp. 21–27.

30. Olsen, F. O. 2009. *Hybrid Laser-Arc Welding.* CRC Press.

31. Zhang, L. J., Zhang, J. X., Wang, R., Yao, W., and Gong, S. L. 2005. Effects of side assist gas on the CO_2 laser welding process of thin stainless plate. *Applied Laser*, Vol. 25, pp. 217–221.

32. Ready, J. F., and Farson, D. F. 2001. *LIA Handbook of Laser Materials Processing*, Laser Institute of America.

33. Shackelford, J. F., and Alexander, W. 2000. *Materials Science and Engineering Handbook* (third edition). CRC Press.

34. Yang, S. L. 2009. Hybrid laser-arc welding of galvanized steels in a gap-free lap joint configuration. Dissertation. Southern Methodist University.

35. Dowden, J. 2009. *The Theory of Laser Materials Processing: Heat and Mass Transfer in Modern Technology* (1st edition). Springer Press.

36. Lu, S. P., Fuji, H., Nogi, K., and Sato, T. 2004. Marangoni convection and weld shape variations in Ar-O_2 and Ar-CO_2 shielded GTA welding. *Material Science Engineering A*, Vol. 380, pp. 290–297.

37. Dong, W. C., Liu, S. P., Li, D. Z., and Li, Y. Y. 2009. Modeling of the weld shape development during the autogenous welding process by coupling welding arc with weld pool. *Journal of Material Engineering and Performance*, pp. 1–9.

38. Smith, A. A. 1970. *CO_2 Welding of Steel* (3rd Edition). The Welding Institute.

39. Glowacki, M. H. 1995. The effects of the use of different shielding gas mixtures in laser welding of metals. *Journal of Physics D: Applied Physics*, Vol. 28, pp. 2051–2059.

40. Grigoruants, A. G. 1997. *Basics of Laser Material Processing*. CRC Press.

41. Xie, J., and Kar, A. 1999. Laser welding of thin sheet steel with surface oxidation. *Welding Journal* 78(10): 343-s to 348-s.

42. Fukuyama, H., and Waseda, Y. 2009. *High-Temperature Measurements of Materials (Advances in Materials Research)*, Springer Press.

43. Zhao, L., Tsukamoto, S., Arakane, G., and Sugino, T. 2009. Influence of oxygen on weld geometry in fibre laser welding. *ICALEO 2009*, pp. 759–765.

44. *Welding Handbook*, Vol. 2. Miami, Fla.: American Welding Society.

45. Jeffus, L. 2002. *Welding Principles and Applications*, fifth edition, Thomson Delmar Learning Press.

46. Zhang, Y. M., and Zhang, S. B. 1999. Observation of the keyhole during plasma arc welding. *Welding Journal* 78(2): 53-s to 58-s.

47. Olsen, F. O. 2009. *Hybrid Laser-Arc Welding.* CRC Press.

WELDING JOURNAL
Instructions and Suggestions for Preparation of Feature Articles

Text
- approximately 1500–3500 words in length
- submit hard copy
- submissions via disk or electronic transmission — preferred format is Mac but common PC files are also acceptable
- acceptable disks include zip, CD, and DVD.

Format
- include a title
- include a subtitle or "blurb" highlighting major point or idea
- include all author names, titles, affiliations, geographic locations
- separate paper into sections with headings

Photos/Illustrations/Figures
- glossy prints, slides, or transparencies are acceptable
- black and white and color photos must be scanned at a minimum of 300 dpi
- line art should be scanned at 1000 dpi
- photos must include a description of action/object/person and relevance for use as a caption
- prints must be a minimum size of 4 in. x 6 in., making certain the photo is sharp
- do not embed the figures or photos in the text
- acceptable electronic format for photos and figures are EPS, JPEG, and TIFF. TIFF format is preferred.

Other
- illustrations should accompany article
- drawings, tables, and graphs should be legible for reproduction and labeled with captions
- references/bibliography should be included at the end of the article

Editorial Deadline
- January issue deadline is November 21
- February issue deadline is December 19
- March issue deadline is January 23
- April issue deadline is February 20
- May issue deadline is March 23
- June issue deadline is April 20
- July issue deadline is May 22
- August issue deadline is June 22
- September issue deadline is July 24
- October issue deadline is August 21
- November issue deadline is September 21
- December issue deadline is October 22

Suggested topics for articles
- case studies, specific projects
- new procedures, "how to"
- applied technology

Mail to:
Mary Ruth Johnsen
Editor, Welding Journal
550 NW LeJeune Road
Miami, FL 33126
(305) 443-9353, x 238; FAX (305) 443-7404
mjohnsen@aws.org